Assimilation of Earth Rotation Parameter observations to constrain and evaluate atmospheric models

Lisa Neef[1] and Katja Matthes[1]

Corresponding author: L.J. Neef, Düsternbrooker Weg 20, D-24105 Kiel, Germany (neef@geomar.de)

[1]Ocean Circulation and Climate Dynamics - Marine Meteorology, Helmholtz Centre for Ocean Research Kiel (GEOMAR), Kiel, Germany.

Abstract. Variability in the Earth's rate of rotation and the orientation of its rotational pole is primarily driven by changes in atmospheric angular momentum on timescales shorter than a few years. This implies that observations of Earth rotation parameters contain information about the dynamics of the atmosphere. It has therefore been proposed to assimilate these parameters into atmosphere and ocean models, as an additional observable constraint for prediction and model evaluation. In this study we test this idea by performing perfect model experiments, assimilating Earth rotation parameters into the Community Atmosphere Model using an Ensemble Adjustment Kalman Filter. This is tantamount to assimilating the global integrals of the wind and surface pressure fields. We show that the assimilation of Earth rotation parameters is only able to reduce error in a model ensemble under very limited conditions. Generally, the assimilation of Earth rotation paramters causes the ensemble filter to diverge because the constraint imposed by the observations is too weak to stop the growth of nonlinearities. It is also found that the assimilation of Earth rotation parameters does not add value to the assimilation of more conventional, localized observations, but actually causes the filter to diverge from the true state because FILL IN REASON. However, including atmospheric angular momentum in an assimilation experiment as evaluated variables can provide a useful measure for the fidelity of an assimilation system where the true state is not known. The results found here could be extended to other cases where integral or averaged observations are assimilated.

1. Introduction

The assimilation of data into numerical models of the atmosphere and ocean has now evolved from its original purpose in numerical weather prediction, to the application in climate modeling. Data assimilatiom methods and codes are now accessible non-experts, in the form of out-of-the-box assimilation toos tools such as the Data Assimilation Research Testbed [*Anderson et al.*, 2009, DART] or the Parallel Data Assimilation Framework [*Nerger and Hiller*, 2013, PDAF].

The evolution of data assimilation algorithms and tools enables us to use various observations of the Earth system to constrain and evaluate climate models. Space geodesy, i.e. the measurement of the figure, position, and geoid of the Earth from satellites, very long baseline interferometry, and satellite and lunar laser ranging, offers a unique source of information about the Earth system.

In particular, it has been found that the angular momenta of the atmosphere and ocean can be observed in terms of anomalies in the Earth's polar orientation and rotation rate, the so-called Earth Rotation Parameters (ERPs). For example, *Neef et al.* [2014] showed that sudden stratospheric warmings are typically preceded by a circa 60 milli-arcsecond wobble in the polar orientation, 3-4 weeks before the warming onset. [Insert another example of how the atmosphere has footprints in the ERPs.]

It makes sense to ask whether more clear connections between observed Earth rotation variations and atmosphere/ocean models can be drawn by formally assimilating these parameters into models. This was done by *Saynisch et al.* [2011, 2010]; *Saynisch and Thomas* [2012], who assimilated the observed ERP timeseris into various ocean model

simulations, found that the observations implied that large adjustments in the model's mass distribution and currents are are necessary in order for the modeled ocean angular momentum to agree with observations. However, those studies did not show how much of this change was due to the addition of the integral observations, nor whether or not the ERP observations actually added information to gridpoint observations that were also assimilated.

It is not clear whether observations like the ERPs can indeed usefully constrain the modeled state, because the ERPs represent integrals of the modeled wind (or current) and mass fields, rather than local quantities. While the prospect of assimilating non-gridpoint observations like ERPs is an exciting possibility, these observations represent integrals of the model state and their assimilation with standard algorithms is therefore not straightforward.

An assimilation algorithm looks for an adjustment to a model that brings it closer to the observations being assimilated. However, even though the resulting model adjustment may improve the fit to the assimilated observations, it will not necessarily bring the modeled state closer to the truth.

It is not sufficient to evaluate the fit between the model and the observations, since the assimilation algorithm is designed to fit the observations. In so-called Observing System Simulation Experiments (OSSEs) a model is used to simulate a "true" state, from which observations are generated and assimilated back into either the same or another model. OSSEs make it possible to evaluate an observation configuration and/or an assimilation technique because the true state is known, and can be directly compared to the analysis model state. In this study we perform OSSEs, using the community data assimilation

facility DART, to evaluate whether ERPs are suited for data assimilation and show some of the difficulties associated with assimilating an integral quantity as a model constraint.

In non-idealized assimilation experiments, it is difficult to judge whether the assimilation of a given set of observations has actually succeeded in bringing the estimated state closer to the truth. Here it is important to compare the assimilated state with independent observations. However, these are often difficult to obtain because different observing systems often don't overlap sufficiently in time and space.

In Section ** we demonstrate how the modeled excitation of Earth rotation variations by the angular momentum of the atmosphere can be used as a measure of the assimilation efficacy, by implementing atmospheric angular momentum as an evaluated but unassimilated observation in DART.

2. Methodology

Assimilation experiments are performed using the Ensemble Adjustment Kalman Filter [*Anderson*, 2001, EAKF] and the Community Atmosphere Model 5 [*Neale et al.*, 2010, CAM5], using the Data Assimilation Research Testbed [*Anderson et al.*, 2009; *Raeder et al.*, 2012, DART].

2.1. Atmospheric Model

CAM5 is run with the finite-volume dynamical core with a $1.9x2.5$ degree lat/lon horizontal resolution, and 30 hybrid-coordinate vertical levels, with a top near 3 hPa. CAM5 forms the atmospheric component of the Community Earth System Model (CESM).

The top three model levels (starting at about 14 hPa) constitute a sort of "sponge" layer, where horizontal diffusion is applied to temperature, vorticity, and divergence in

order to absorb vertically propagating planetary waves. The diffusion has been tuned in order to give a reasonable strength of the stratospheric polar night jets [*Neale et al.*, 2010].

2.2. Observations

Two types of observations are assimilated: a set of idealized "local" observations from radiosondes (section 2.2.2) and observations of the angular momentum of the atmosphere (section 2.2.1).

2.2.1. Atmospheric Angular Momentum Observations

We generate the atmospheric angular momentum (AAM) of the model state at each observation time, using the following non-dimensional equations derived by *Barnes et al.* [1983]:

$$\chi_1(t) = \frac{1.608}{\Omega\,(C-A')}\left[0.684\Omega\Delta\mathbf{I}_{13}(t)+\Delta h_1(t)\right] \quad (1)$$

$$\chi_2(t) = \frac{1.608}{\Omega\,(C-A')}\left[0.684\Omega\Delta\mathbf{I}_{23}(t)+\Delta h_2(t)\right] \quad (2)$$

$$\chi_3(t) = \frac{0.997}{\Omega C_m}\left[0.750\Omega\Delta\mathbf{I}_{33}(t)+\Delta h_3(t)\right], \quad (3)$$

where χ_1 and χ_2 represent the angular momentum vector components defined by the intersection of the equator with the 180°W and 0° meridians, respectively, and χ_3 reprents the axial component. The $\mathbf{I}_{ij}$ terms represent the components of the atmospheric inertia tensor:

$$I_{13} = -\int R^2\cos\phi\sin\phi\cos\lambda\,dM \quad (4)$$

$$I_{23} = -\int R^2\cos\phi\sin\phi\sin\lambda\,dM \quad (5)$$

$$I_{33} = \int R^2\cos^2\phi\,dM, \quad (6)$$

and the h_i terms the relative angular momentum (due to winds) in each direction:

$$h_1 = -\int R\,[u \sin\phi \cos\lambda - v \sin\lambda]\,dM \tag{7}$$

$$h_2 = -\int R\,[u \sin\phi \sin\lambda + v \cos\lambda]\,dM \tag{8}$$

$$h_3 = \int Ru \cos\phi dM. \tag{9}$$

$R = 6371.0$ km is the radius of the Earth, $\Omega = 7.292115 \times 10^{-5}$rad/s the average rotation rate, and $g = 9.81\text{m/s}^2$ is the acceleration due to gravity. $C = 8.0365 \times 10^{37}\text{kgm}^2$ and $A = 8.0101 \times 10^{37}\text{kgm}^2$ are the axial and next-largest principal moments of inertia of the solid Earth, and $C_m = 7.1236 \times 10^{37}\text{kgm}^2$ is the principal inertia tensor component of the Earth's mantle [*Gross*, 2009].

Note that the zonal integration in the axial AAM terms [(6) and (9)] weights all longitudes equally. In practice, this means that mass anomalies tend to cancel one another out in the zonal integral, with the result that the axial mass excitation (6) is usually several orders of magnitude smaller than the axial wind excitation (9) [*Barnes et al.*, 1983].

Nearly the opposite is true for the equatorial AAM terms [(4)-(5) and (7)-(8)], where stronger zonal asymmetry in the wind and mass fields leads to a larger global integral. For these functions, the mass terms [(4) and (5)] typically outweigh the wind terms [(7) and (8)] by a few factors [*Barnes et al.*, 1983].

As they are defined here, χ_1 largely reflects surface pressure variations over the oceans, and χ_2 over the continents. Consequently, χ_2 has a pronounced annual cycle due to the yearly appearance of the Siberian High [*Dobslaw et al.*, 2010], and tends to show strong negative anomalies in the month preceding a sudden stratospheric warming [*Neef et al.*, 2014]. χ_1, in contrast, has much weaker subseasonal to annual variations, in part because surface pressure variations over the ocean tend to be evened out by corresponding

displacements of the ocean surface (the so-called "inversted barometer" effect, e.g. *Salstein and Rosen* [1989]).

In reality, of course, we don't measure the atmospheric angular momentum but rather the variations in the Earth rotation parameters that are excited by the above angular momentum functions. Therefore in practice one would have to rotate the observed polar motion parameters into equivalent equatorial angular momentum components, convert observed length-of-day anomalies into corresponding axial angular momentum, and subtract out the excitation of each parameter that is due to other components of the Earth system. For the purposes of this study, it is sufficient to assimilate the three AAM components directly, since we are performing perfect model experiments and therefore know the true state.

Nevertheless, it is conceptually helpful to transform the axial AAM function χ_3 into corresponding anomalies in the length of a day (ΔLOD), which is done using the following relationship:

$$\Delta\mathrm{LOD} \;=\; \Delta\chi_3 \times \mathrm{LOD}_0, \tag{10}$$

where LOD_0 denotes the nominal length-of-day (86400s).

For our experiments, observations of χ_1, χ_2, and χ_3 are generated every 24 hours, reflecting the observation frequency of the real ERP series released by Earth rotation services.

2.2.2. Idealized Radiosonde Observations

In order to evaluate the assimilation of Earth rotation variations, we need to compare it to the assimilation of conventional, spatially-distributed observations such as are normally assimilated in the generation of atmospheric reanalysis [*Dee*, 2005] or weather prediction

models (CITE). Since compiling all the available observations is a complicated task in itself, we simulate the conventional observation grid using an idealized, global grid of radiosonde-like observations.

The horizontal grid of the radiosonde observations is shown in Figure 1.

How many RS observations per day?

2.2.3. Synthetic GPS-RO Observations

In Section **??** we investigate the usefulness of AAM observations as an evaluated variable when spatially-localized observations are assimilated.

2.3. Data Assimilation System

Assimilation is performed using the Data Assimilation Research Testbed (DART), an open-source, community facility that makes ensemble data assimilation available for any model, using any observations. It is available online at `www.image.ucar.edu/DAReS/DART`. DART includes a variety of assimilation algorithms in the Ensemble Kalman Filter family. Here we use the so-called Ensemble Adjustment Kalman Filter (EAKF) of *Anderson* [2001].

The EAKF is called a deterministic ensemble filter because it solves for the updated state error statistics deterministically using Bayes' theorem, and then adjusts the forecast ensemble accordingly. In contrast, so-called stochastic filters like the Ensemble Kalman Filter [*Evensen*, 2003; **?**] first updates the forecast ensemble with perturbed observations (to reflect the observation uncertainty), and then computes the updated state uncertainty from the updated ensemble.

When an observation is made, we have a prior estimate of the observation predicted by the ensemble ($y_{b,i}$, where b denotes the *background* estimate and i denotes an individual

ensemble member), and the observation itself, y_{obs}. Bayes' theorem states that the conditional probability distribution function (PDF) of the estimated observation value, given the prior ensemble estimate on the one hand and the actual measurement on the other, is the product of their respective PDFs. The resulting joint PDF has an updated variance σ_a^2 (where a denotes the update or *analysis*) given by:

$$\sigma_a^2 = \left[\left(\sigma_b^2\right)^{-1} + \left(\sigma_{\text{obs}}^2\right)^{-1} \right]^{-1}, \tag{11}$$

where σ_b^2 is the prior error variance of the observation implied by the ensemble, σ_{obs}^2 is the error variance of the observation itself (i.e. the measurement error).

The updated ensemble mean of the joint probability distribution is then given by

$$\langle y_a \rangle = \sigma_a^2 \left(\frac{\langle y_b \rangle}{\sigma_b^2} + \frac{y_{\text{obs}}}{\sigma_{\text{obs}}^2} \right), \tag{12}$$

and the updated observation-space value of each ensemble member is given by

$$y_{a,n} = \left(\frac{\sigma_a^2}{\sigma_b^2} \right) \left(y_{b.n} - \langle y_b \rangle \right) + \langle y_a \rangle , \tag{13}$$

i.e. a linear transformation of the ensemble members about the updated mean such that (17) is satisfied by the ensemble [*Anderson and Collins*, 2006].

Practically, of course, we don't update the observations implied by the ensemble, but rather the *state* of each ensemble member, i.e. the wind, surface pressure, and temperature fields. The state vector of each ensemble member, $\mathbf{x}_n$, is updated simply by projecting the observation space update $\Delta y_n = y_{n,a} - y_{n,b}$ onto the individual state components x_i via linear regression:

$$\Delta x_{i,n} = \left(\frac{c_{x_i y}}{\sigma_b^2} \right) \Delta y_n, \tag{14}$$

where $c_{x_i y}$ represents the prior covariance between the state component x_i and the observation y.

Because the EAKF adjusts the ensemble based on the expected error reduction, it is called a stochastic ensemble filter. In contrast, so-called stochastic filters, such as the well-known Ensemble Kalman Filter (EnKF), adjust the forecast ensemble first with perturbed upservations, and then compute the resulting error distribution from the ensemble.

The novelty of ensemble assimilation algorithms is that the covariance c_{x_iy} and the prior and posterior variances σ_b^2 and σ_a^2 are computed dynamically, using the ensemble of model states:

$$c_{x_iy} = \langle (x_i - \langle x_i \rangle)\,(y - \langle y \rangle) \rangle \tag{15}$$

$$\sigma_b^2 = \left\langle (y_{b,n} - \langle y_b \rangle)^2 \right\rangle \tag{16}$$

$$\sigma_a^2 = \left\langle (y_{a,n} - \langle y_a \rangle)^2 \right\rangle, \tag{17}$$

which means that they change in time and are updated at the observation times. In a successful ensemble assimilation system, these continually-updated covariances should reflect the true error statistics of the model system. If this is not the case, the ensemble filter will most likely diverge, a condition where the uncertainty predicted by the ensemble underestimates the true error.

2.4. Perfect-model experiments

We perform so-called Observing System Simulation Experiments (OSSEs), wherein a model is used to generate a "true state", and observations are generated from this simulation with known error statistics, then assimilated back into the model. OSSEs are designed to show how much information can truly be recovered by assimilation when all model and observation errors are known and controlled.

2.4.1. True State and Ensemble Generation

[Insert description of how we generated the true state.] All assimilation runs were performed with an 80-member ensemble. The ensemble is generated by selecting the 1 January restart files from an 80-year simulation of CAM5, and then running a year of assimilation of the synthetic radiosonde observations (Section 2.2.2).

2.4.2. Output Diagnostics

Our main evaluation diagnostics are the square error between the simulated true state and the ensemble mean

$$E_M = (\langle x_i \rangle - x_{i,t})^2 \tag{18}$$

and the ensemble variance about its mean:

$$S = \frac{1}{N} \sum_{n=1}^{N} (\langle x_{i,n} \rangle - x_t)^2 , \tag{19}$$

where $x_{i,n}$ represents a component of the state vector in the ensemble, $x_{i,t}$ the corresponding component in the truth, and $\langle \cdot \rangle$ represents the ensemble mean, as in section 2.3.

In order to evaluate whether the ensemble is an accurate representation of the true uncertainty, we test whether the truth can be considered a sample of the probability distribution represented by the ensemble. *Huntley and Hakim* [2009] and *Murphy* [1988] pointed out that this is the case when

$$[\![E_M]\!] = \frac{N+1}{N} [\![S]\!], \tag{20}$$

where the square brackets represent spatial averages.

A second way to quantify whether the ensemble and the truth come from the same probability distribution is to compute rank histograms [*Hamill*, 2001, and references therein] A rank histogram is generated by ordering the values of the ensemble at each point in

the state space, and then finding the rank of some verification value on this list. In our case, we simply use the true state as the verification, since it is known. The rank of the verification is then counted up over many different assimilation times and state space points; we then generate a histogram of these ranks. If the truth comes from the same PDF as the ensemble, the rank histogram should be nearly flat. If the truth is a frequent outlier of the PDF represented by the ensemble, the rank histogram will by concave. A convex rank histogram indicates an ensemble whose spread is so large that the truth is usually the central rank.

2.4.3. Experiment Overview

Four assimilation experiments are performed, summarized in Table 1: In the first (NoDA), the 80-member ensemble is allowed to evolve without any assimilation. Only the three AAM components are assimilated (12-hourly) in experiment AAM. In experiment RST, the temperature observations from the idealized radiosonde grid are assimilated 6-hourly. In experiment RST+AAM, both the radiosonde temperatures and the AAM components are assimilated. Experiments NoDA and AAM were integrated for two months, 1 January to 28 February 2009. Exeperiments RST and RST+AAM were only integrated for the first 31 and 17 days of this period, respectively, because this amount of integration time was found to be sufficient to give the results presented in this study.

3. AAM as an Assimilation Variable

3.1. Error reduction in observation space

Our first comparison of the experiments in Table 1 is in terms of the three components of AAM [(1)-(3)]. Figure 2 compares the prior ensemble to the true state for each of the three AAM components, and for experiments NODA, AAM, RST, and RST+AAM. With

no assimilation (first column), the three AAM values of the ensemble spread rapidly about the truth, saturating after about a month. As the different observational constraints are applied (columns 2-4), we can see that the constraint on the modeled AAM components increases.

Assimilating the three global AAM components (second column) brings the ensemble of all three AAM functions close to their true values. This indicates that the EAKF is able to adjust the dynamical state of each ensemble member such that the observed AAM is satisfied. This suggests that the assimilation of the AAM components offers a useful constraint, but it does not yet tell us whether or not the error in these variables (i.e. column 1 of Fig. 3) is indeed reduced. This will be investigated more closely in Section 3.2.

The reduction in the spread of the ensemble around the truth is almost as good as when local radiosonde temperatures with global coverage are assimilated (experiment RST, third colum). The fit to the true AAM functions is best when both local temperatures and AAM are assimilated (experiment RST+AAM, fourth column). In the space of the AAM functions, then, it looks as though the assimilation of AAM is able to constrain the state similarly to the constraint offered by the local observations, and adds value when these two observation types are combined (Fig. **??**(d)).

However, success in fitting the assimilated variables is not sufficient for the success of an assimilation system, because it does not guarantee that the state variables themselves are closer to the true state. This will be investigated in the next section.

Thought: this might not be the best way to present things. Don't really want to lead the reader down the bunny trail of thinking that the fit to obs is sufficient, when it isn't. What is a better way to write this section?

3.2. State-space diagnostics

3.2.1. Error growth without assimilation

Before examining the error in the ensemble when observations are assimilated, it is useful to examine how the ensemble in our assimilation system spreads relative to the true state when no observations are assimilated, because this shows us what information can actually be gained from assimilating. Figure 3(a) compares the mean square error between the ensemble mean and the true state (MSE hereafter) to the variance of the ensemble after it has been scaled by $(N+1)/N$, as in (20). The first row shows MSE and ensemble variance for the zonal wind, as a function of vertical level and time, averaging zonally and meridionally. The second row of plots compares the MSE and the scaled ensemble spread in the surface pressure, over latitude and time, averaging zonally.

For the zonal wind, both the error and the ensemble variance begin to grow first around 250 hPa, which is near the altitudes of the extratropical jets. The growth of the scaled ensemble variance here is largely commensurate with the growth of the MSE. The relative agreement between the growth of the true error and the ensemble spread isn't surprising, since in our case the"truth" is actually a realization of the same model that produced the ensemble.

At the surface (Fig. 3b-c) error growth happens first at high latitudes, especially in the Northern Hemisphere. Here the scaled ensemble variance somewhat underestimates the

MSE. Do we have an explanation for this? Or are they "close enough"? – check after comparing to rank histograms.

The error in the zonal wind field also becomes underestimated after abount a month, when the ensemble mean MSE shows large errors at the highest model levels (near the "sponge" layer, see Section 2.1), which is not captured by the ensemble variance. Again, need an explanation for this.

As stated in the introduction, the goal of ensemble assimilation is to generate an ensemble that captures the true uncertainty in the estimated state, given the observations, which also means that the true state should, be a sample of the PDF represented by the ensemble. To test whether our ensemble achieves this, we construct a rank histogram.

Figure **??**a shows the rank histogram for surface pressure in the NODA experiment, counting over all points in the model grid, and assimilation days 10-20. The histogram is mildly concave, indicating that the true state is somewhat more likely to be lower or higher than all ensemble members. This means that the ensemble spread in this experiment is somewhat too small, but by and large the truth can still be considered a sample of the ensemble. Need to verify that the RH for zonal and meridional wind is qualitatively similar.

In order for the assimilation experiments of the next section to be successful, they should achieve two goals: (1) to decrease the true error, and (2) to maintain an ensemble that is as or more representative of the true error as in the NoDA experiment.

3.2.2. Assimilation of AAM

Figure **??**b shows the surface pressure rank histogram for experiment AAM DA, i.e. after assimilating the three global excitation functions (1)-(3). Clearly, the assimilation

has made the rank histogram much more concave, which means that the truth is now a very frequent outlier of the PDF represented by the ensemble. The rank histograms for the wind fields, not shown here, are qualitatively similar. This in turn suggests that the model ensemble has clustered more closely together in terms of the surface pressure, even while it is well spread out around the observed AAM (Fig. **??**, second column).

Figure **??**a-b shows the MSE and scaled ensemble variance in the surface pressure, as in Fig. 3b-c, but for the AAM DA experiment. Figure **??**c-d shows the difference in MSE and scaled ensemble variance between AAM DA and No DA (positive values indicating larger values in AAM DA). When the AAM components are assimilated, MSE (Fig. **??**a) grows more or less as in the No DA case (Fig. 3c), but the difference between then (Fig. **??**c) shows that the assimilation has decreased the error in some places, and increased it in others. In contrast, the ensemble variance (Figure **??**b,d) has decreased everywhere when the AAM components are assimilated.

3.3. Evolution of the Covariance Field

It was seen above that the ensemble filter is able to update the state more or less correctly at the beginning of the assimilation, actually makes the error between the ensemble mean and the true state worse later on in the assimilation period. The degree to which each variable field is changed as the assimilation progresses depends on the covariances between local variables (in our case, winds or surface pressure) and the global AAM functions (15). The covariance $c_{x_i y}$ is estimated for each state variable x_i and each observation y by the statistics of the model ensemble. A point in the model state can have a large covariance with the global AAM either if it has a large variance, or if it has a large correlation to the global AAM, or both.

4. Can Earth rotation observations add value?

The previous sections showed that the assimilation of AAM observations can reduce error in the modeled wind and pressure fields, as long as the ensemble spread has not reached its saturation level. Thus it makes sense to test whether the assimilation of AAM is more successful if the AAM functions are assimilated together with (more conventional) spatially localized observations to keep the ensemble spread from growing.

In terms of the AAM functions themselves [Fig. **??**(d)] we saw that combining regularly-spaced observations with the AAM observations yielded an overal better-constrained state. However, we found that the same is not true in terms of the model state variables. [Insert figure showing that adding AAM to local temperature observations increases the error while decreasing the spread.]

Figure 8 is similar to Fig. 5, but now comparing experiment RST to experiment RST+AAM. Again, we see that the consequence of adding AAM components as an assimilation variables is that the filter diverges, and here the effect is much stronger than in the basic experiment (Fig. 5).

5. AAM as an evaluation variable

GPS-RO measurements have been shown to add a high amount of information to numerical weather forecasts (Bonavita, 2013), due to their low systematic errors and high vertical resolution. It was shown by (Wang et al., 2013) that GPS-RO data give an unprecedented look into the vertical structure of the atmosphere because of their high vertical resolution, in this case showing a warming trend in the tropopause inversion layer that would not have been observed otherwise.

6. Summary

In this study we tested the efficacy of assimilating Earth rotation parameters, which represent changes in the atmospheric angular momntum and therefore integrals of the atmospheric wind and pressure fields. This was done by performing perfect model assimilation experiments wherein the three components of the global atmospheric angular momentum were assimilate, with and without complementary meteorological observations.

It may be assumed that the assimilation integral quantities can lead to an overall improvement of a modeled atmosphere or ocean state. Indeed, this was done by *Saynisch et al.* [2010, 2011]; *Saynisch and Thomas* [2012] for Earth rotation parameters and by [CITE other examples of integral constraints]. However, we found that an improved state estimate is difficult to achieve when integral-type observations are assimilated, because the assimilation decreases ensemble spread without improving the accuracy of the ensemble.

It was found that the assimilation of the three components of AAM is able to decrease state error in an ensemble of simulations, but only during the initial spin-up period when both the spread of the ensemble and the true error are quite small As both the error and spread grow, it becomes too easy to fit the observed AAM without actually bringing the ensemble closer together.

In Kalman filter-based data assimilation, the state is adjusted most strongly in regions where the covariance between the state components and each observation is highest, which means that it depends both on the model spread at each point in the state vector, as well as the correlation of that point to the observation. Thus points with a large ensemble spread recieve a stronger adjustment than points with a smaller spread, which may not always reflect the true situation (i.e. points with a large true error are not adjusted enough), but

as long as the correlation is estimated correctly, the adjustment will be made in the right direction.

The correlations should be estimated accurately if the model and observation operator are perfect and the ensemble is large enough (three conditions that are guaranteed in our experiments). However, our experiments showed that the modeled correlations between state components and the AAM observations become less and less accurate as the assimiliation progresses. This means that the ensemble becomes less and less represenative of the true error in time, i.e. that the truth and the forecast ensemble are no longer members of the same probability distribution.

These results lead to the possible conclusion that angular momentum oscillations might better constrain the state when assimilated in conjunction with local state observations that keep the spread in the ensemble small. However, we found that in this case, the additional assimilation of angular momentum degrades the analysis. Fill in the reason for this when I really understand it.

There exists a potential way to assimilate integral observations, based on the study of *Dirren and Hakim* [2005], but applying this method is doubtful to offer improvements upon the assimilation of other available observations, such as GPS-RO measurements. Need to explain why I think so.

We have found that the real usefulness of Earth rotation observations is that they can measure the fidelity of a data assimilation system because they offer a way to quantify the global state error in terms of three simple components that all reflect different things.

Acknowledgments. The computations discussed in this study were performed at the Deutsches KlimaRechenZentrum (DKRZ) in Hamburg, Germany. We are grateful to

Nancy Collins for help with porting DART to the DKRZ supercomputer. This work has been performed within the Helmholtz-University Young Investigators Group NATHAN, funded by the Helmholtz-Association through the President's Initiative and Networking Fund, the Helmholtz Centre for Ocean Sciences Kiel, the Helmholtz Centre for Geosciences Potsdam, and the Freie Universität Berlin.

References

Anderson, J., T. Hoar, K. Raeder, H. Lui, N. Collins, R. Torn, and A. Avellano (2009), The data assimilation research testbed: A community facility, *Bull. Am. Met. Soc.*, pp. 1283–1296, doi:10.1175/2009BAMS2816.1.

Anderson, J. L. (2001), An ensemble adjustment filter for data assimilation, *Mon. Wea. Rev.*, *129*, 2884–2903.

Anderson, J. L., and N. Collins (2006), Scalable implementations of ensemble filter algorithms for data assimilation, *J. Atmos. Ocean. Technol.*, *24*, 1452–1463.

Barnes, R., R. Hide, F.R.S., A. White, and C. Wilson (1983), Atmospheric angular momentum fluctuations, length-of-day changes and polar motion, *Proc. Roy. Soc. London*, *387*, 31–73.

Dee, D. P. (2005), Bias and data assimilation, *Quart. J. Roy. Meteorol. Soc.*, *131*(613), 3323–3343, doi:10.1256/qj.05.137.

Dirren, S., and G. J. Hakim (2005), Toward the assimilation of time-averaged observations, *Geophys. Res. Lett.*, *32*(4), L04,804, doi:10.1029/2004GL021444.

Dobslaw, H., R. Dill, A. Grötsch, A. Brzezinski, and M. Thomas (2010), Seasonal polar motion excitation from numerical models of atmosphere, ocean, and continental

hydrosphere, *J. Geophys. Res.*, *115*, 10,406, doi:10.1029/2009JB007127,2010.

Evensen, G. (2003), The ensemble Kalman filter: theoretical formulation and practical implementation, *Ocean Dynamics*, *53*, 343–367.

Gross, R. S. (2009), Earth rotation variations - long period, in *Geodesy, Treatise on Geophysics*, edited by T. Herring, pp. 239–294, Elsevier.

Hamill, T. M. (2001), Interpretation of Rank Histograms for Verifying Ensemble Forecasts, *Monthly Weather Review*, *129*(3), 550–560, doi:10.1175/1520-0493(2001)129⟨0550:IORHFV⟩2.0.CO;2.

Huntley, H. S., and G. J. Hakim (2009), Assimilation of time-averaged observations in a quasi-geostrophic atmospheric jet model, *Climate Dynamics*, *35*(6), 995–1009, doi:10.1007/s00382-009-0714-5.

Murphy, J. (1988), The impact of ensemble forecasts on predictability, *Quarterly Journal of the Royal Meteorological Society*, *114*, 463–493.

Neale, R. B., C.-c. Chen, P. H. Lauritzen, D. L. Williamson, A. J. Conley, A. K. Smith, M. Mills, and H. Morrison (2010), Description of the NCAR Community Atmosphere Model (CAM 5.0), *National Center for Atmospheric Research Tech. Rep.*, (NCAR/TN-486+STR.), 268.

Neef, L., S. Walther, K. Matthes, and K. Kodera (2014), Observations of Stratospheric Sudden Warmings in Earth Rotation Variations, *J. Geophys. Res.*, in press.

Nerger, L., and W. Hiller (2013), Software for ensemble-based data assimilation systemsImplementation strategies and scalability, *Computers & Geosciences*, *55*, 110–118, doi:10.1016/j.cageo.2012.03.026.

Raeder, K., J. L. Anderson, N. Collins, T. J. Hoar, J. E. Kay, P. H. Lauritzen, and R. Pincus (2012), DART/CAM: An ensemble data assimilation system for CESM atmospheric models, *J. Clim.*, doi:10.1175/JCLI-D-11-00395.1, in press.

Salstein, D. A., and R. D. Rosen (1989), Regional contributions to the atmospheric excitations of rapid polar motions, *J. Geophys. Res.*, *94*, 9971–9978.

Saynisch, J., and M. Thomas (2012), Ensemble Kalman-Filtering of Earth rotation observations with a global ocean model, *J. Geodyn.*, *62*, 24–29, doi:10.1016/j.jog.2011.10.003.

Saynisch, J., M. Wenzel, and J. Schröter (2010), Assimilation of earth rotation parameters into a global ocean model: length of day excitation, *J. Geodesy.*, *85*, 67–73.

Saynisch, J., M. Wenzel, and J. Schröter (2011), Assimilation of earth rotation parameters into a global ocean model: excitation of polar motion, *Nonlin. Proc. Geophys.*, *18*, 581–585.

References

Table 1. Overview of assimilation experiments performed.

Experiment name	Assimilated Quantities	Integration Time (Days)
NODA	none	81
AAM	χ_1, χ_2, ΔLOD	81
RST	Radiosonde temperatures	31
RST+AAM	Radiosonde temperatures, χ_1, χ_2, ΔLOD	17
GPS-RO	CHAMP-like GPS-RO refractivities	FILL IN

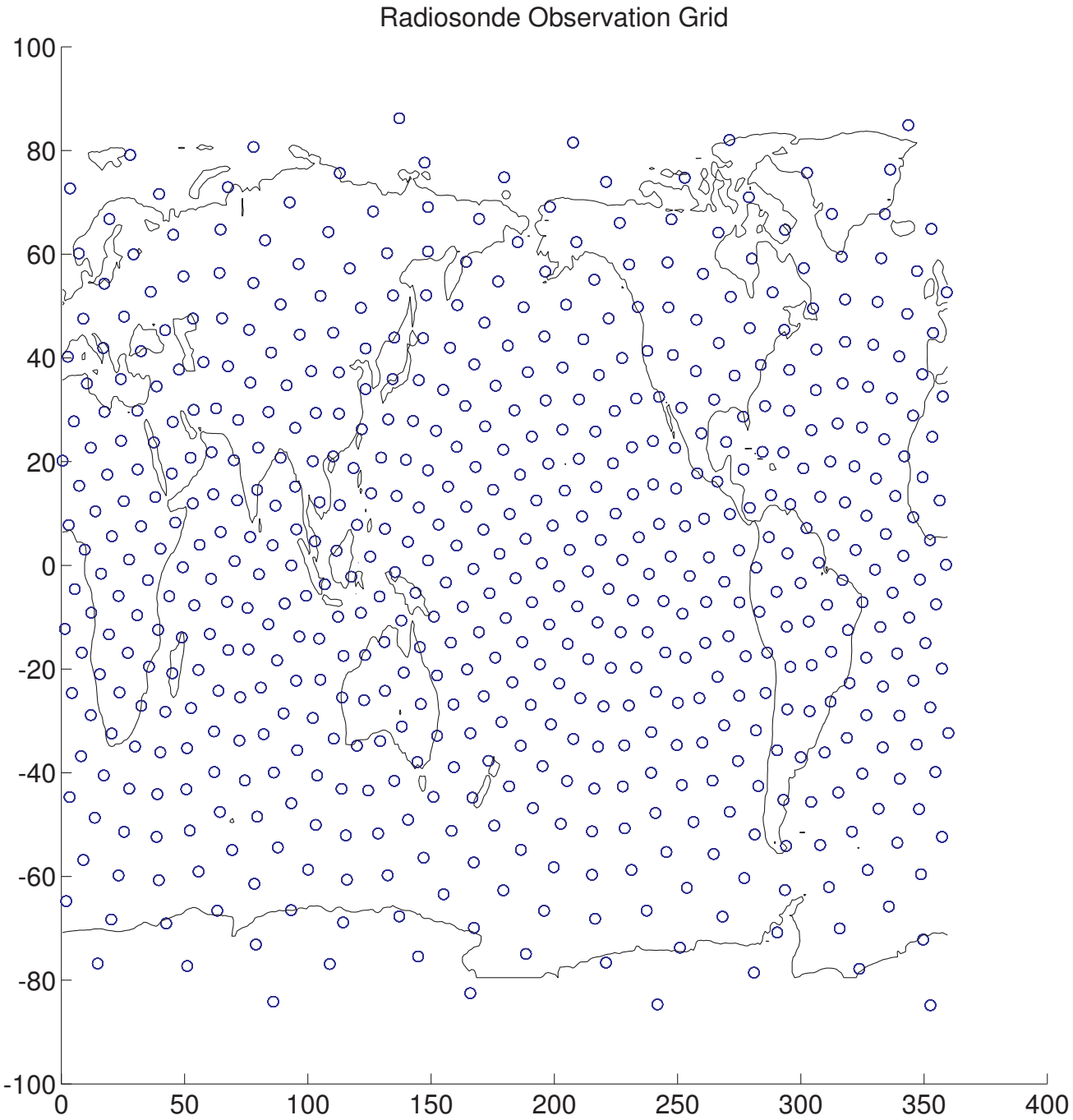
Radiosonde Observation Grid
100
80
60
40
20
0
-20
-40
-60
-80
-100
0
50
100
150
200
250
300
350
400

Figure 1.

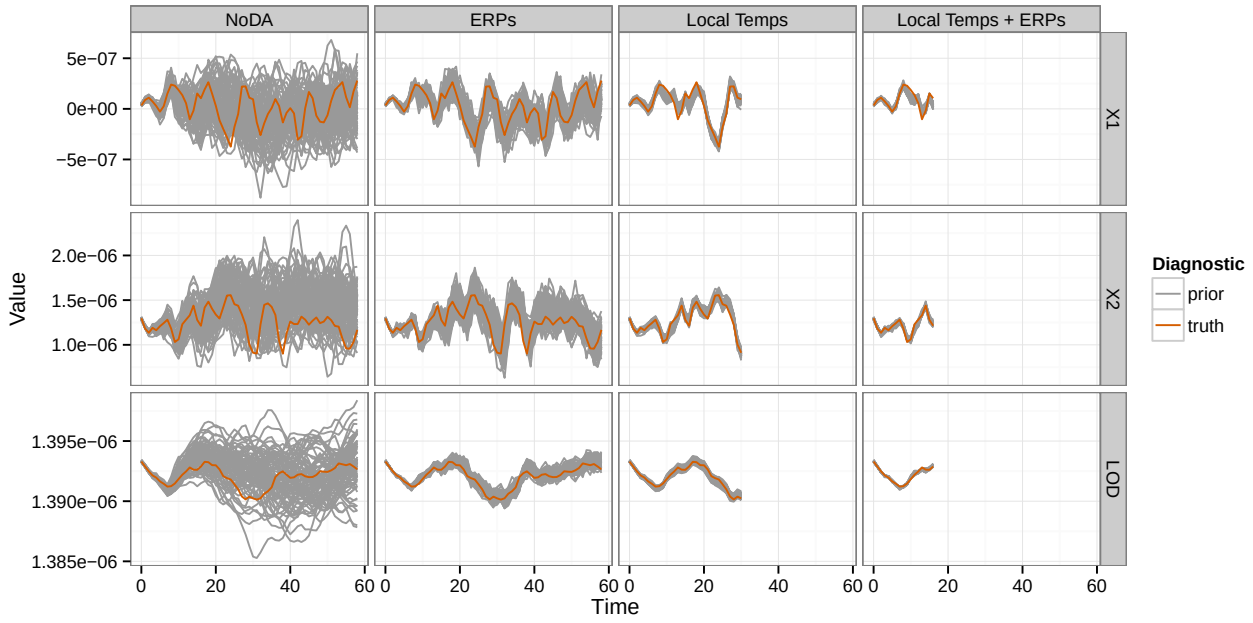

Figure 2. The DART prior ensemble (gray) compared to the true state (orange) in terms of assimilation time and each of the three angular momentum functions [(1)-(3), (10)]. The columns compare the four experiments summarized in Table 1.

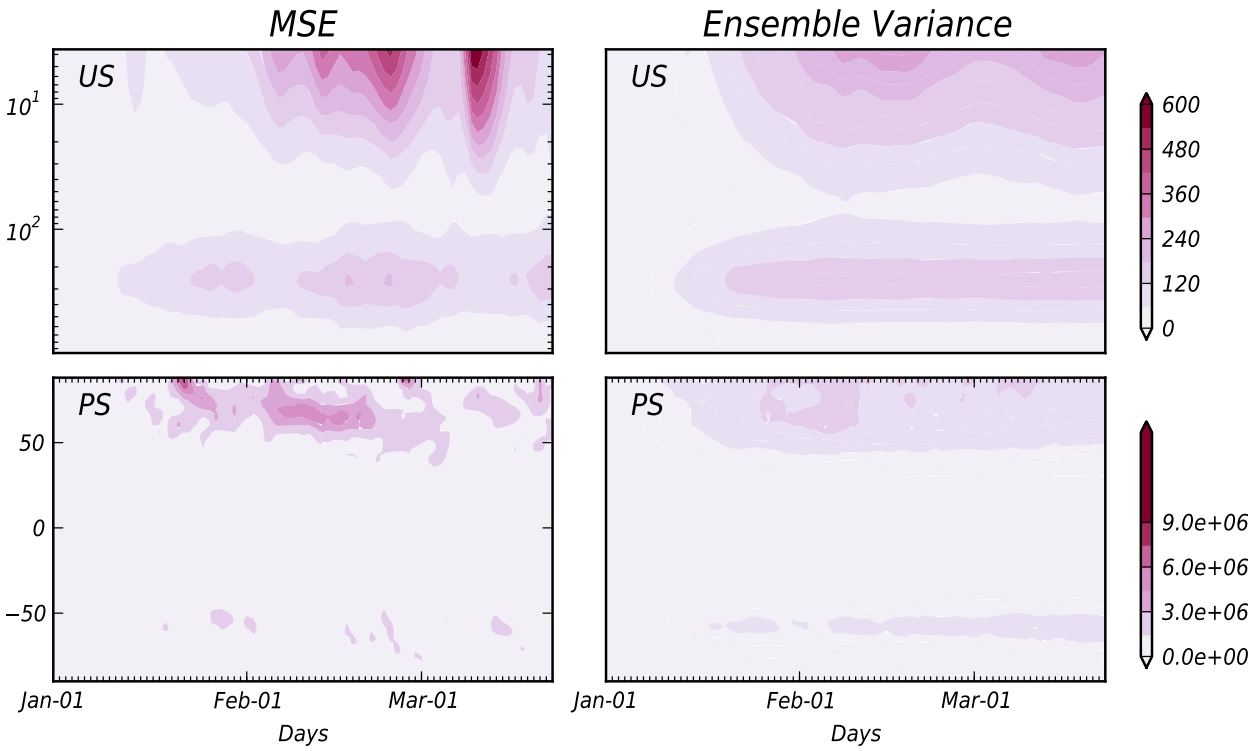

Figure 3. Top row: The mean square error in the ensemble mean zonal wind field as a function of vertical level and time (left), compared to the corresponding scaled ensemble spread (as in (20), center), for the NoDA experiment. Bottom row: as in the first row, but for surface pressure, and plotting over latitude and time. Changes: add letter labels.

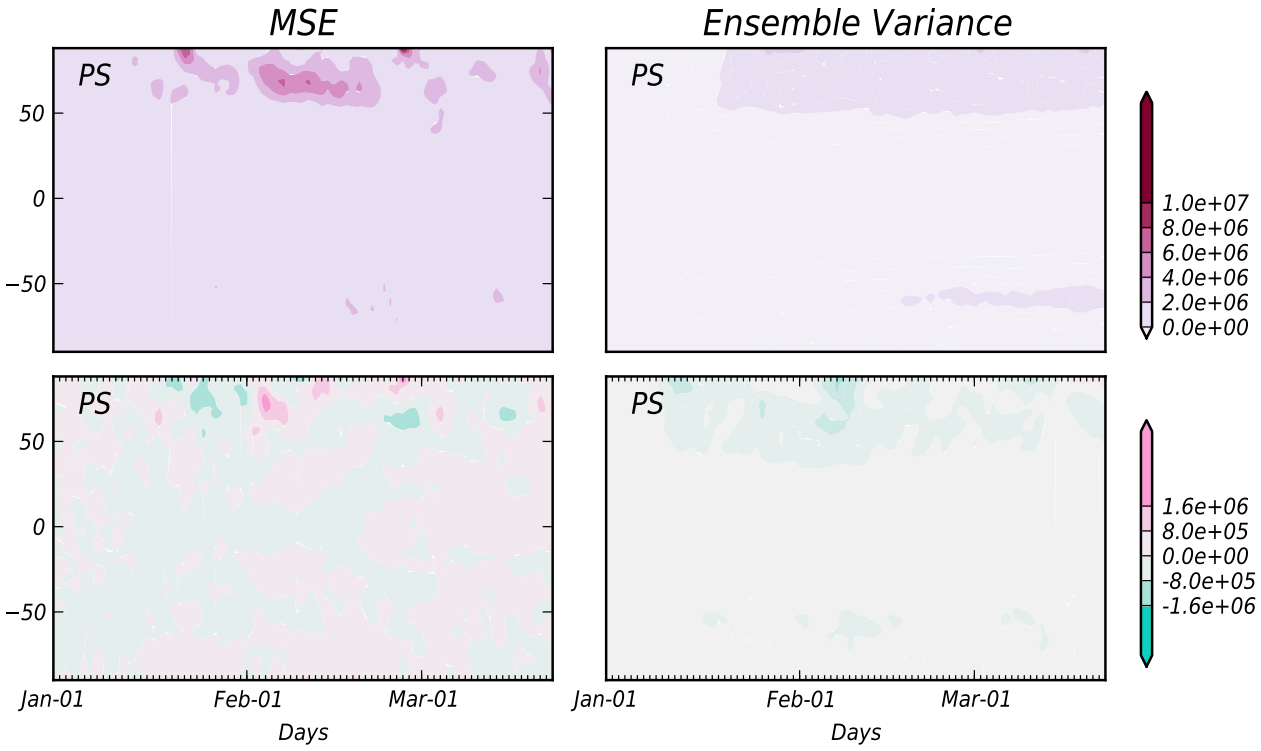

Figure 4. Top row: The mean square error in the ensemble mean surface pressure field, and a function of latitude and time (left), compared to the corresponding scaled ensemble spread (as in (20), center), for experiment AAM. Bottom row: The difference between the surface pressure mean square error and ensemble spread fields in the AAM experiment, relative to the NoDA experiment. To do: add letter labels here to make it easier to compare panels.

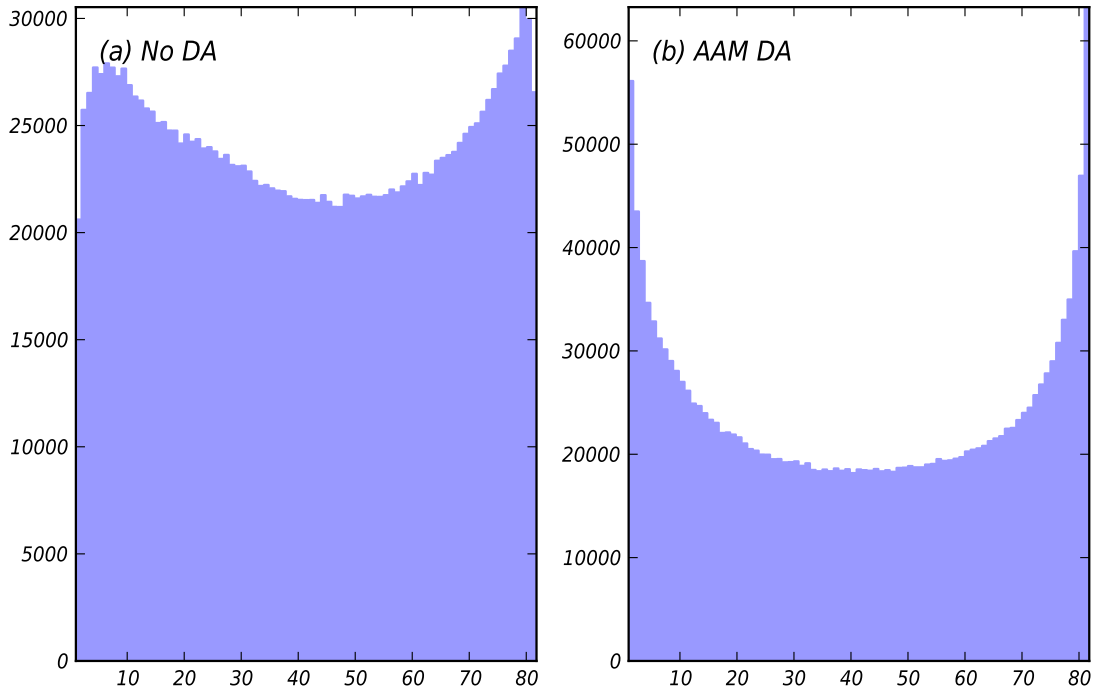

Figure 5. Rank histograms for surface pressure, counting over assimilation days 10-20 for (a) the NODA experiment, and (b) the AAM experiment.

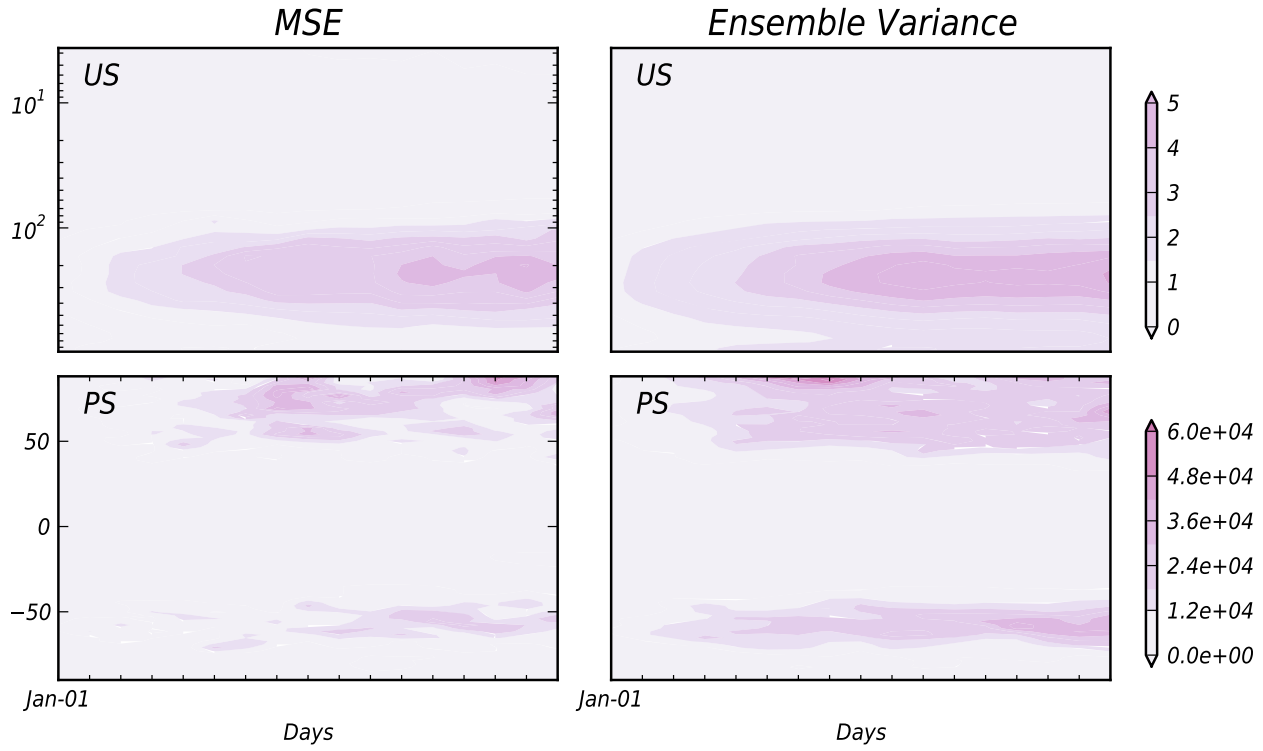

Figure 6. As in Figs. 3 and 4, but for experiment RST (assimilating radiosonde temperatures only).

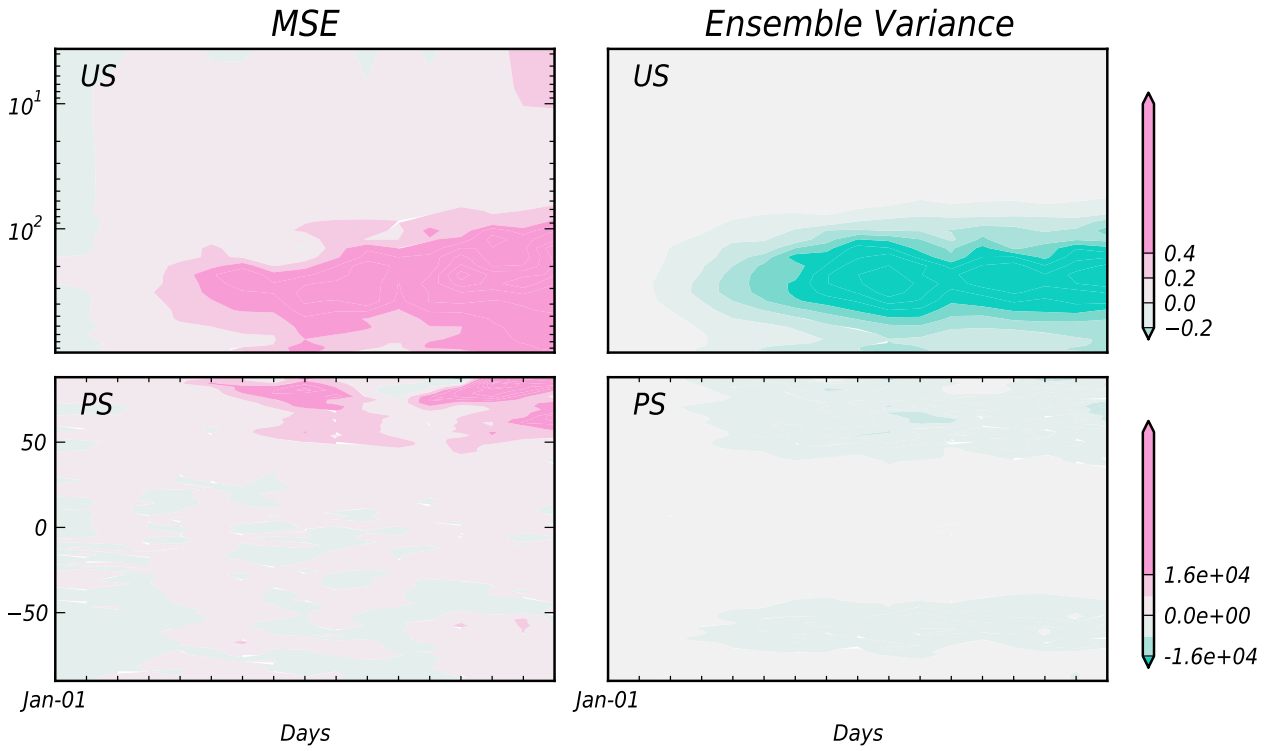

Figure 7. As in Fig. **??**, but now showing the differences between experiments AAM+RST and RST (positive values mean larger error or spread in experiment AAM+RST relative to RST).

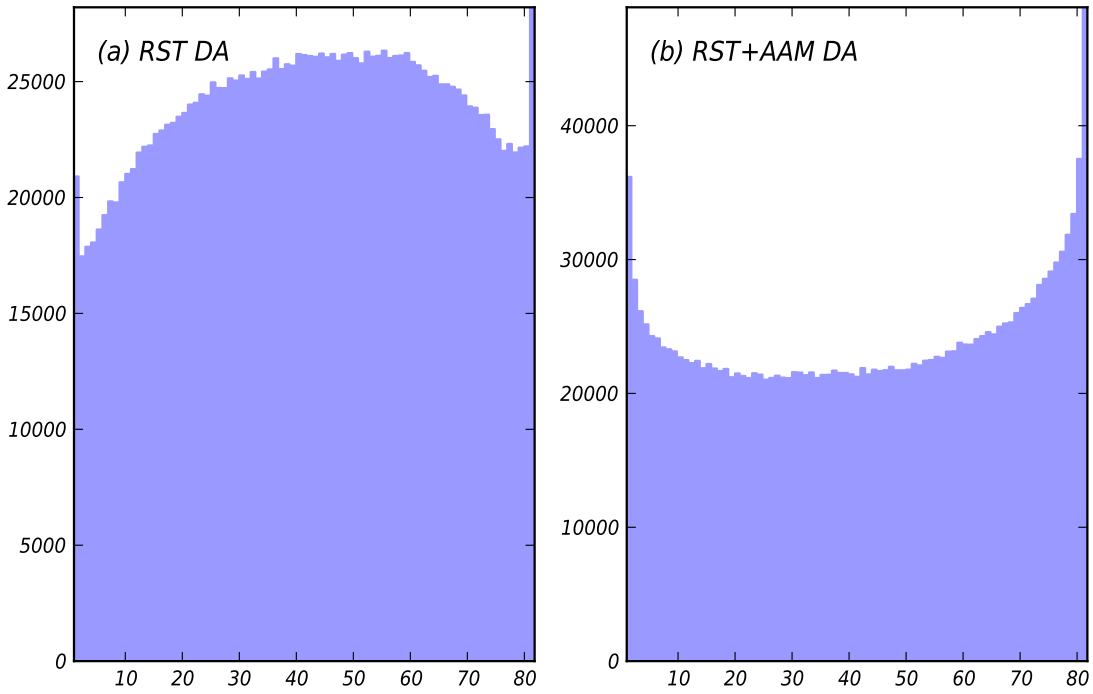

Figure 8. Replace this with rank histograms.